

Unique Lamellar Sodium/Potassium Iron Oxide Nanosheets: Facile Microwave-Assisted Synthesis and Magnetic and Electrochemical Properties

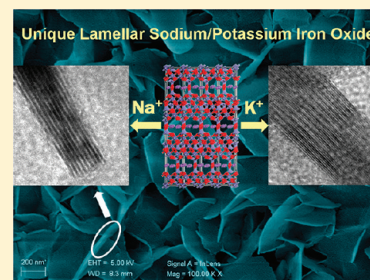
Liheng Wu, Hongbin Yao, Bo Hu, and Shu-Hong Yu*

Division of Nanomaterials and Chemistry, Hefei National Laboratory for Physical Sciences at Microscale, Department of Chemistry, National Synchrotron Radiation Laboratory, University of Science and Technology of China, Hefei, Anhui 230026, P. R. China

S Supporting Information

ABSTRACT: Unique lamellar sodium/potassium iron oxide nanosheets consisting of two-dimensional iron oxide building blocks have been synthesized by microwave-assisted heating the suspension of iron(II) sulfate, sodium thiosulfate, and sodium/potassium hydroxide within 5 min. These lamellar iron oxide building blocks are separated by intercalated sodium/potassium ions, which possess typical ferromagnetic properties due to the magnetic anisotropy of the lamellar iron oxide. Owing to their layered feature, these nanosheets with a high Brunauer–Emmett–Teller (BET) surface area could allow fast Li-ion diffusion, and thus the preliminary investigations on their electrochemical properties have been carried out, which indicate potential applications of these lamellar nanosheets as anode materials for high-performance lithium-ion batteries. Moreover, this facile microwave-assisted synthesis strategy will open a new route to prepare other lamellar metal oxide nanomaterials with unique architectures and multifunctionalities.

KEYWORDS: microwave-assisted process, lamellar nanosheets, ferromagnetic, electrochemistry, lithium-ion battery



1. INTRODUCTION

Lamellar nanomaterials with specific architectures and novel properties have received increasing attention for both scientific and technological interests in recent years.^{1–4} Among these layered nanomaterials, lots of artificial lamellar structures containing both inorganic and organic components have been synthesized, e.g., layered polydiacetylene/silica mesostructures,⁵ ultrathin CoSe₂–amine nanobelts,⁶ and tungstate-based inorganic–organic nanobelts.⁷ Layered double hydroxides (LDHs), as another kind of important lamellar structure, have attracted much attention as well due to their layered feature and highly tunable interlayer composition.^{8–12} Besides, intense research efforts have been made on the synthesis and characterization of layered transition metal oxides. For instance, layered niobates have been reported to show great potentials in semiconductors, catalysts, sensors, and so on.^{13–16} Layered Li_xMn_yO₂¹⁷ and cobalt-substituted manganese oxide¹⁸ have been synthesized with improved capacity and cycling performance as lithium-battery electrodes. Superconductivity has been found in the layered Na_xCoO₂·yH₂O compound with two-dimensional CoO₂ layers and intercalated Na⁺ and H₂O molecule layers.² The layered Ca₃Co₄O₉ nanosheet,¹⁹ a new kind of layered electrode material, has also been investigated, showing a high and reversible specific capacity.

However, as for the layered metal oxides, most of them were prepared at an elevated temperature of more than 700 °C through solid-state reactions and required a long reaction time. Compared to conventional synthetic methods, microwave-

assisted synthesis has been demonstrated to be more facile and environmentally friendly, which can significantly shorten the reaction time.²⁰ By taking advantage of this novel method, lots of inorganic nanostructures have been prepared, including nanoparticles,^{21–24} nanocables,²⁵ nanorings,²⁶ and nanorods.²⁷ Up until now, lamellar metal oxide nanosheets have not been synthesized through this fast and facile method.

Herein, we report a facile and fast microwave-assisted method for synthesis of unique lamellar sodium/potassium iron oxide nanosheets consisting of two-dimensional iron oxide building blocks separated by the intercalated sodium/potassium ions. The obtained nanosheets exhibit ferromagnetic properties due to the existence of iron oxide layers in the lamellar structures. Moreover, the preliminary investigations on electrochemical performance of these nanosheets as anode materials are presented, indicating potential applications in high-performance lithium-ion batteries.

2. EXPERIMENTAL SECTION

2.1. Materials. Iron(II) sulfate heptahydrate (FeSO₄·7H₂O), sodium thiosulfate pentahydrate (Na₂S₂O₃·5H₂O), sodium hydroxide (NaOH), potassium hydroxide (KOH), and lithium hydroxide monohydrate (LiOH·H₂O) were all purchased from Sinopharm Chemical Reagent Co., Ltd. and used as received without further purification.

Received: May 15, 2011

Revised: July 26, 2011

Published: August 05, 2011

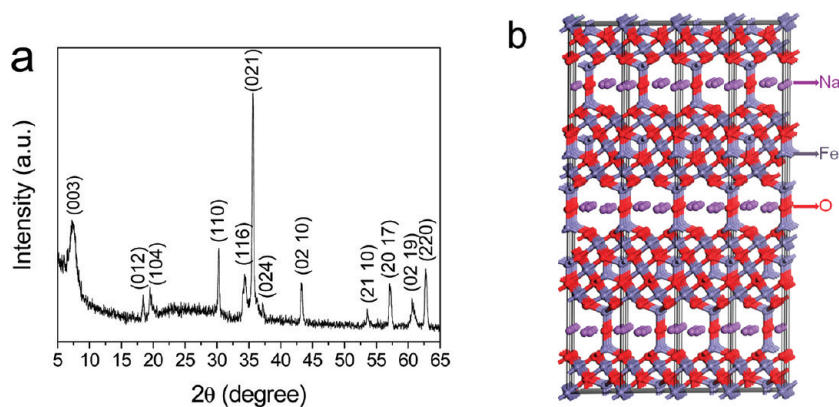


Figure 1. (a) XRD pattern of the obtained sodium iron oxide nanosheets synthesized under microwave irradiation at 180 °C for 5 min. (b) Crystal structure of $\text{Na}_{2.4}\text{Fe}_{10.99}\text{O}_{16.03}$ viewed perpendicular to the c axis. The pink, red, and gray balls correspond to Na, O, and Fe atoms, respectively.

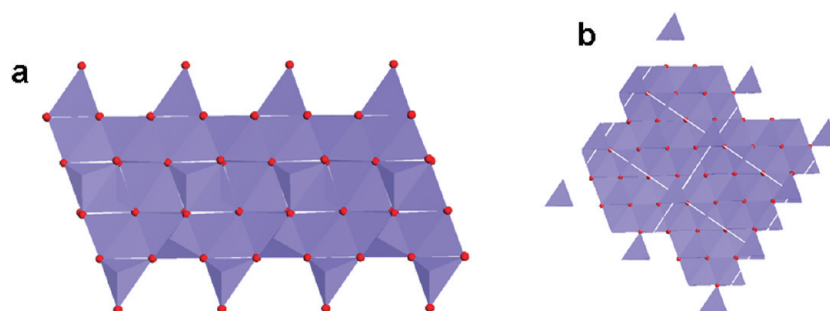


Figure 2. Polyhedron depiction of iron oxide crystal structures. (a) Building blocks in sodium iron oxide and (b) Fe_3O_4 . The two-dimensional iron oxide building blocks can be viewed as fragments that cut from the Fe_3O_4 .

2.2. Preparation of Sodium/Potassium Iron Oxide Nanosheets. In a typical synthesis, 2 mmol of iron(II) sulfate heptahydrate ($\text{FeSO}_4 \cdot 7\text{H}_2\text{O}$, 0.556 g) and 1 mmol of sodium thiosulfate pentahydrate ($\text{Na}_2\text{S}_2\text{O}_3 \cdot 5\text{H}_2\text{O}$, 0.248 g) were dissolved in 15 mL of deionized water (DIW), and then 25 mmol of sodium hydroxide (NaOH, 1 g) was added to form dark green suspension. After magnetic stirring for about 5 min, 5 mL of the suspension was transferred into the microwave vessel. Here, the microwave system utilized was a CEM Discover Microwave Synthesizer (CEM Corporation, USA). The suspension was heated to 180 °C by microwave at the power of 75 W under magnetic stirring and maintained for 5 min. Dark precipitates were collected after fast air-cooling to room temperature and then washed by deionized water and ethanol several times with centrifugation. Potassium ion substituted layered nanosheets were obtained by replacing 25 mmol of NaOH with the same molar amount of KOH (1.403 g) while maintaining the amount of other reagents constant. Octahedral Fe_3O_4 nanoparticles were obtained by substituting 25 mmol of lithium hydroxide monohydrate ($\text{LiOH} \cdot \text{H}_2\text{O}$, 1.049 g) for 25 mmol of NaOH.

2.3. Characterization. X-ray diffraction (XRD) data were recorded by a Rigaku DMax- γ A diffractometer with a monochromatic Cu K α radiation ($\lambda = 1.5418 \text{ \AA}$). The morphology of the synthesized products was characterized on a Zeiss Supra 40 scanning electron microscope (SEM) at an accelerating voltage of 5 kV. Transmission electron microscopy (TEM) and high-resolution transmission electron microscopy (HRTEM) measurements were performed on a Hitachi 7650 transmission electron microscope and JEOJ-2010 transmission electron microscope at an accelerating voltage of 200 kV, respectively. XPS spectra of the products were obtained using an ESCALAB MK II spectrometer. Elemental analysis of the nanosheets was performed by

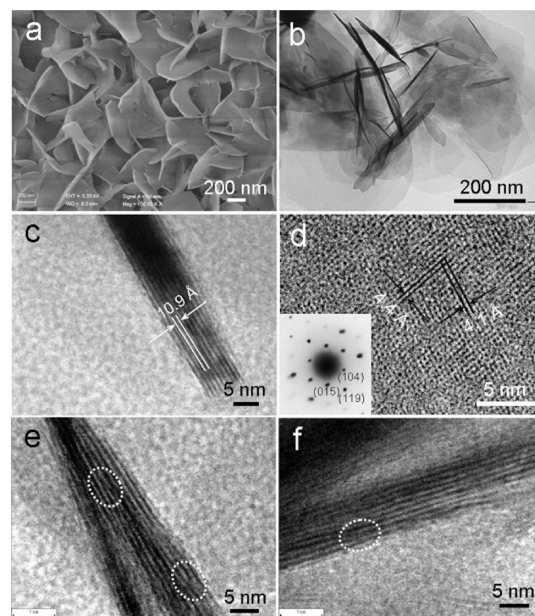


Figure 3. (a) SEM image and (b) TEM image of the as-prepared $\text{Na}_{2.4}\text{Fe}_{10.99}\text{O}_{16.03}$ nanosheets via microwave-assisted synthesis at 180 °C for 5 min. HRTEM images of (c) a vertical and (d) a planar $\text{Na}_{2.4}\text{Fe}_{10.99}\text{O}_{16.03}$ nanosheet (inset is the SAED pattern). (e) and (f) HRTEM images of different vertical $\text{Na}_{2.4}\text{Fe}_{10.99}\text{O}_{16.03}$ nanosheets. Dislocations in the layered structures are marked by the dashed ellipses.

inductively coupled plasma (ICP) atomic emission spectroscopy (AES) using an AtomsScan Advantage spectrometer. Fourier transform infrared

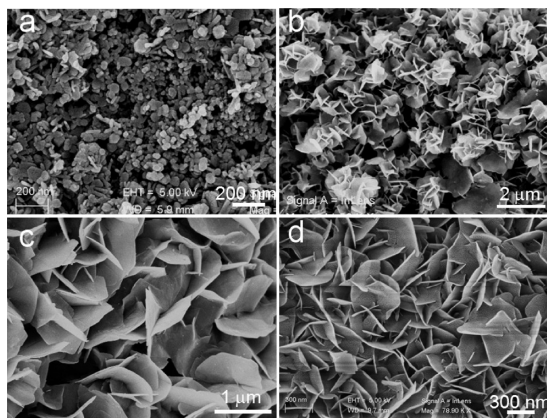


Figure 4. SEM images of (a) the precursors and SEM images of the samples prepared at 180 °C under microwave irradiation for different reaction time: (b) 1 min, (c) 2 min, and (d) 5 min, respectively.

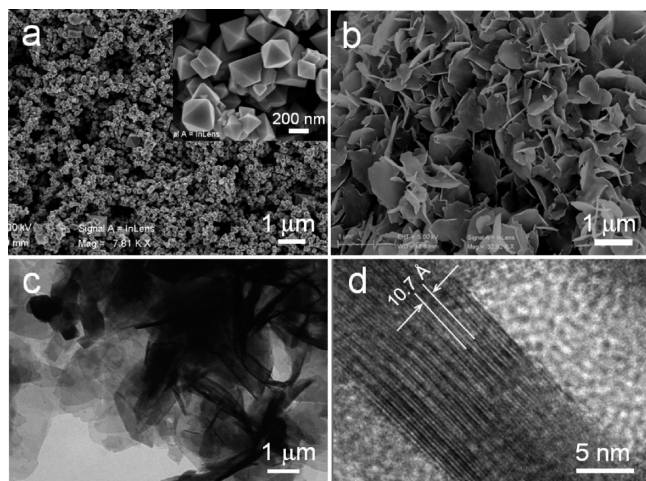


Figure 5. (a) SEM images of the Fe_3O_4 nanoparticles synthesized using LiOH instead of NaOH under microwave irradiation at 180 °C for 5 min. (b) SEM and (c) TEM images of the potassium iron oxide nanosheets synthesized by replacing NaOH with KOH under microwave irradiation at 180 °C for 5 min. (d) HRTEM image of a vertical potassium iron oxide nanosheet.

(FT-IR) spectra in a range of 400–4000 cm^{-1} were measured on a Bruker Vector-22 FT-IR spectrometer using the solid olefin pellet technique. Thermal gravimetric analysis (TGA) was carried out using a Perkin-Elmer Diamond TG/DTA thermal analyzer at a heating rate of 5 °C under nitrogen. Superconducting quantum interference device (SQUID) measurements were carried out by using a Quantum Design MPMS XL magnetometer.

2.4. Electrochemical Measurements. The working electrodes were prepared by mixing the nanosheets, acetylene black (AB), and poly(vinylidene fluoride) (PVDF) at the weight ratio of 70:20:10 onto a copper foil. The electrode sheets were dried at 120 °C in a vacuum oven. Using a porous polypropylene membrane (Celgard 2400) as the separator, coin cells were assembled in an argon-filled glovebox for electrochemical measurements. The electrolyte was 1 M LiPF_4 in an ethylene carbonate/dimethyl carbonate (EC-DMC) mixture (w/w 1:1). Li metal foils were used as the counterelectrodes. The cells were galvanostatically charged and discharged at a current density of 50 mA g^{-1} over a range of 0.2–2.8 V.

3. RESULTS AND DISCUSSION

The phase of the as-synthesized product was first investigated. The XRD pattern of sodium iron oxide in Figure 1a shows that all the diffraction peaks can be indexed to a hexagonal symmetry of $\text{Na}_{2.4}\text{Fe}_{10.99}\text{O}_{16.03}$ (space group: $R\bar{3}m$, $a = 5.947 \text{ \AA}$, $c = 35.83 \text{ \AA}$; JCPDS card No. 84-1924). It can be clearly seen that the pattern exhibits a strong peak located in the low-angle region (ca 7.3°) with a d value of 11.9 Å, indicating the formation of lamellar structures. The crystal structure of $\text{Na}_{2.4}\text{Fe}_{10.99}\text{O}_{16.03}$ is shown in Figure 1b. The sodium iron oxide is composed of two-dimensional iron oxide building blocks which are connected by the Fe–O–Fe bonds. Sodium ions are localized in pores between the layered iron oxide building blocks to neutralize the negative charge existing in the iron oxide layer. The two-dimensional iron oxide building blocks in sodium iron oxide can be considered as fragments of Fe_3O_4 shown in Figure 2, in which the iron(II) or iron(III) ions are coordinated by four oxygen atoms to form regular tetrahedron structures or by six oxygen atoms to form regular octahedron structures. However, elemental analyses determined by inductively coupled plasma (ICP) atomic emission spectroscopy (AES) revealed that the Na/Fe molar ratio of the sample was about 2.20:10.99, indicating less Na elements in product compared with the ideal crystal of the $\text{Na}_{2.4}\text{Fe}_{10.99}\text{O}_{16.03}$. Moreover, FT-IR spectra of the product provided evidence for the existence of OH groups (see Supporting Information Figure S1b). These results can be attributed to the Fe–OH groups existing in the defective sites of the low crystalline lamellar

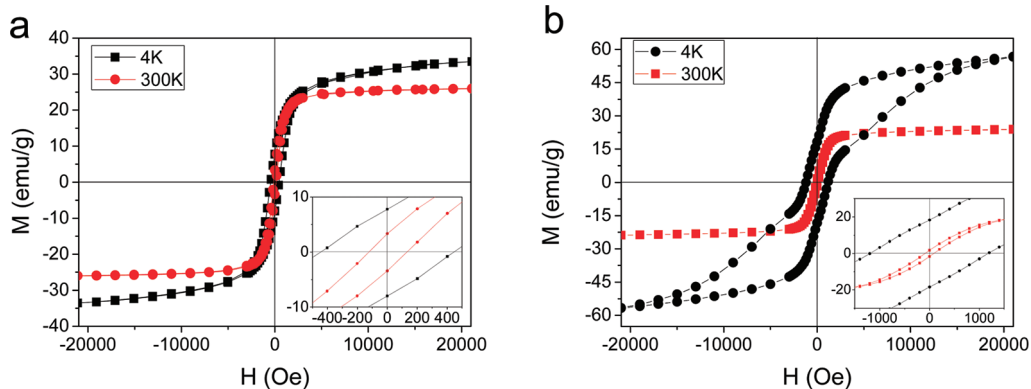


Figure 6. Magnetic hysteresis loops of the as-synthesized (a) sodium and (b) potassium iron oxide layered nanosheets measured at 4 and 300 K. The inset represents the magnified view, showing the remanent magnetization and coercivity.

iron oxide nanosheets synthesized under mild conditions. The presence of Fe–OH groups could explain the lower content of sodium ions in the obtained nanosheets as well. The TGA curves also confirmed the existence of Fe–OH groups which results in the weight loss process in the range of 160–320 °C (Figure S2, Supporting Information).

The scanning electron microscopy (SEM) image in Figure 3a shows the typical morphology of the as-synthesized $\text{Na}_{2.4}\text{Fe}_{10.99}\text{O}_{16.03}$ nanosheets, which was assembled from thin nanosheets into a three-dimensional flower-like architecture with an edge length of more than 500 nm in both dimensions. The dark regions suggest the vertical nanosheets, while the light regions correspond to the horizontal or gradient ones as shown in TEM image Figure 3b. A typical HRTEM image taken on a vertical nanosheet was collected to confirm the layered structure of the product. Figure 3c clearly shows the multilayered structures of $\text{Na}_{2.4}\text{Fe}_{10.99}\text{O}_{16.03}$ nanosheets, the distance between which can be evaluated to be about 10.9 Å, which is in agreement with that detected by XRD. A typical HRTEM taken on a planar sheet is shown in Figure 3d. The fringe spacings are about 4.1 and 4.4 Å, corresponding to those for the (015) and (104) planes, respectively. Some edge and screw dislocations are found in nanosheets, as shown in Figures 3e and 3f. The formation of these dislocations could be related with the nonstoichiometric molar ratio of Na and Fe caused by the existence of Fe–OH groups in the nanosheets.

The reaction time dependent morphological change of sodium iron oxide nanosheets was characterized and shown in Figure 4. Thin nanosheets with similar morphology and lamellar structures can be obtained under microwave irradiation for only 1 min (Figure 4b, and see Supporting Information

Figure S3). With prolonging the reaction time to 5 min, the sodium iron oxide nanosheets became bigger and had better crystallinity (Figure 4d). This rapid growth process well demonstrates the facile and fast characteristic of the microwave-assisted synthesis.

Compared with sodium ions, lithium ions with smaller ionic radius cannot favor the formation of similar layered structures. Octahedral nanoparticles rather than nanosheets were synthesized by substituting LiOH for NaOH during the synthesis procedure (Figure 5a), which were confirmed to be pure Fe_3O_4 by the XRD pattern (see Supporting Information Figure S4) (JPCDS card No. 19-0629). However, very similar nanosheets can be obtained if using KOH instead. Figures 5b and 5c show the typical SEM and TEM images of as-prepared nanosheets, respectively. The XRD pattern of the sample shows great similarity to that of the layered $\text{Na}_{2.4}\text{Fe}_{10.99}\text{O}_{16.03}$ nanosheets (see Supporting Information Figure S5a,b), except for the emergence of the diffraction peak of (009) planes located at about 26.4° , indicating obviously improved crystallinity of the products compared with the prepared $\text{Na}_{2.4}\text{Fe}_{10.99}\text{O}_{16.03}$ nanosheets. The HRTEM image in Figure 5d taken on a vertical nanosheet also indicates that those lamellar nanosheets were better crystallized with fewer defects. According to the results of elemental analysis determined by inductively coupled plasma (ICP) atomic emission spectroscopy (AES), the molar ratio of Na:K:Fe was about 0.06:2.24:10.99. The very small amount of Na element in the sample is attributed to the utilization of $\text{Na}_2\text{S}_2\text{O}_3 \cdot 7\text{H}_2\text{O}$ in the reaction under reducing conditions, and thermogravimetric measurement indicated the smaller amount of OH groups in the nanosheets (see Supporting Information Figure S2), which could account for the fewer crystal defects and better crystallinity of the K-substituted nanosheets.

Owing to the existence of two-dimensional iron oxide building blocks in nanosheets, the magnetic properties of as-synthesized layered sodium/potassium iron oxide nanosheets were investigated by the superconducting quantum interference device (SQUID) measurements. Figure 6 displays the magnetization (M) versus magnetic field (H) curves of nanosheets. From M – H curves, it is observed that both of the two samples possess typical ferromagnetic properties, indicating enhanced magnetic anisotropy of those unique lamellar nanosheets compared with Fe_3O_4 nanoparticles.²⁸ The coercivity (H_c) and saturation magnetization (M_s) for layered potassium iron oxide nanosheets at 4 K are 1175 Oe and 56.7 emu g^{-1} , respectively, which are much larger than those for sodium iron oxide nanosheets ($H_c = 443 \text{ Oe}$, $M_s = 33.5 \text{ emu g}^{-1}$). The differences between the two similar

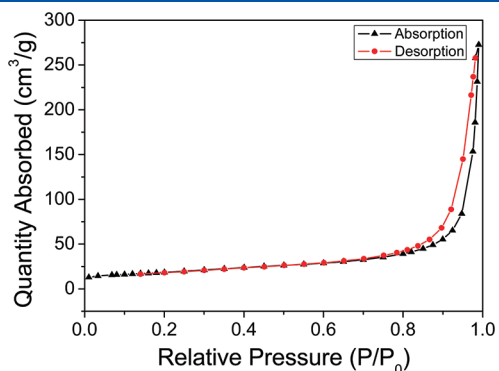


Figure 7. Nitrogen adsorption (\blacktriangle) and desorption (\bullet) isotherms of the as-prepared $\text{Na}_{2.4}\text{Fe}_{10.99}\text{O}_{16.03}$ nanosheets shown in Figure 1 at 77 K.

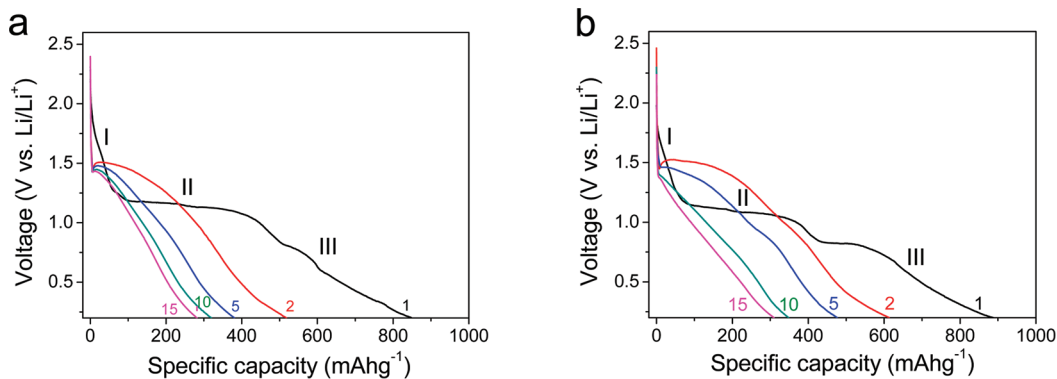


Figure 8. Discharge curves for (a) sodium and (b) potassium iron oxide nanosheets cycled at the rate of 50 mA g^{-1} between 2.8 and 0.2 V vs Li/Li^+ .

structures can be ascribed to their different crystallinity and basal spacings.^{29–31}

To investigate the specific surface area of the $\text{Na}_{2.4}\text{Fe}_{10.99}\text{O}_{16.03}$ nanosheets, Brunauer–Emmett–Teller (BET) nitrogen-sorption measurements were performed at 77 K, and the adsorption–desorption isotherms of these nanosheets were collected (Figure 7). The BET surface area of the overall nanosheets was calculated to be $64.4 \text{ m}^2/\text{g}$. The high surface area of these lamellar metal oxide nanosheets can be conducive to their potential electrochemical applications. Furthermore, nanosized transition metal oxides,^{32–35} including Fe_3O_4 nanoparticles,^{36,37} have been demonstrated to be promising electrode

materials for high-performance lithium-ion batteries. Besides, the lamellar nature of the as-synthesized nanosheets may allow a fast Li-ion diffusion during the Li-ion insertion/extraction. Thus, the preliminary lithium-battery performances of these unique lamellar nanosheets are worth investigating.

The electrochemical performances of the obtained nanosheets were tested by cycling the cells at the constant rate of $50 \text{ mA} \cdot \text{g}^{-1}$ in the potential range of 0.2–2.8 V versus Li/Li^+ . The sodium and potassium iron oxide nanosheets exhibit similar electrochemical properties, as shown in Figure 8. The first discharge curves for both samples can be divided into three regions (I, II, and III). The first one (I) is related to the diffusion of Li ions into the lamellar structures.¹⁹ The second region (II) with the plateau at about 1.1 V and the third region (III) reflecting the continuous voltage drop to 0.2 V could be attributed to the formation of Li_2O and the reduction of iron oxide, which are very similar to those for iron oxide anode materials.^{36,37} Both sodium and potassium iron oxide nanosheets have a relatively large initial discharge capacity of $849 \text{ mAh} \cdot \text{g}^{-1}$ and $888 \text{ mAh} \cdot \text{g}^{-1}$, respectively. After the second discharge measurement, the previous plateau disappeared, and these nanosheets exhibited poor electrochemical stability as shown in Figure 9. After 15 cycling discharge–charge measurements, the discharge capacity dropped significantly to about $300 \text{ mAh} \cdot \text{g}^{-1}$. To make the samples better crystallized for better lithium-ion battery performance, removing the hydroxyl groups in the nanosheets was carried out by annealing. After annealing at $500 \text{ }^\circ\text{C}$ for 3 h, the morphologies of the products changed negligibly (see Supporting Information Figure S6),

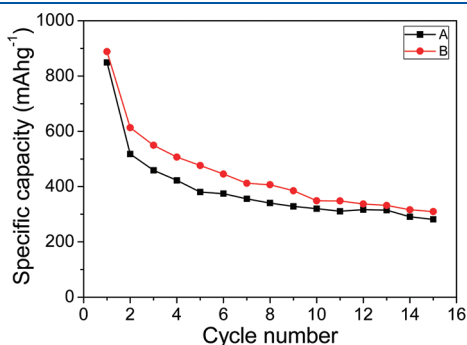


Figure 9. Variation in discharge capacity vs cycle number for (a) sodium and (b) potassium iron oxide nanosheets.

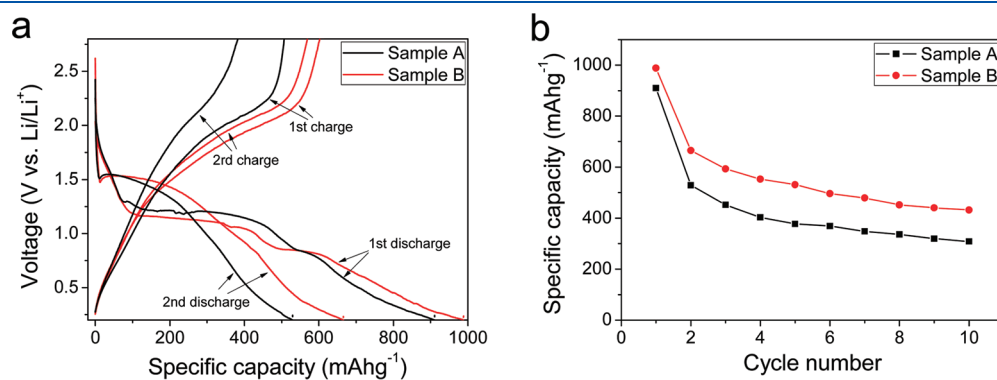


Figure 10. Electrochemical performance of the annealed sodium iron oxide nanosheets (Sample A) and potassium iron oxide nanosheets (Sample B) as anode electrodes in Li battery. (a) First and second charge–discharge voltage profiles for those nanosheets cycled at the rate of $50 \text{ mA} \cdot \text{g}^{-1}$ between 2.8 and 0.2 V vs Li/Li^+ . (b) Variation in discharge capacity vs cycle number for those nanosheets.

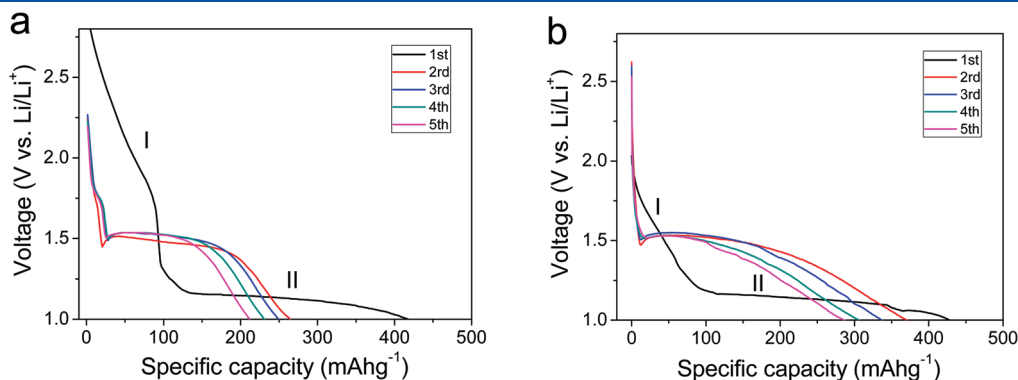


Figure 11. Discharge curves for (a) sodium and (b) potassium iron oxide nanosheets cycled at the rate of $50 \text{ mA} \cdot \text{g}^{-1}$ between 2.8 and 1.0 V vs Li/Li^+ .

and their XRD patterns remained almost the same except for the contraction of the layered structures (see Supporting Information Figure S7). The first and second discharge—charge curves of the annealed samples are shown in Figure 10a. The discharge capacities for both samples indeed enhanced, of which the initial capacity for sodium and potassium iron oxide nanosheets is 910 and 988 mAh·g⁻¹, respectively. However, the clear plateaus in the first discharge curves vanished again in the forthcoming cycles, and the stability of the electrode materials did not improve much, as shown in Figure 10b. XPS spectra of the annealed potassium iron oxide nanosheets (sample B) after the initial discharge showed a sharp Li 1s peak centered at 55.6 eV, indicating the formation of Li₂O (see Supporting Information Figure S8), which corresponded to the reactions in the second and third regions. The XRD pattern of sample B after initial lithium storage also indicated that the layered feature of the nanosheets was destructed (see Supporting Information Figure S9).

Actually, if we did the cyclic measurement between 2.8 and 1.0 V, we also found the irreversibility of the reaction in region II, which is clearly shown in Figure 11. The lamellar structure of the nanosheets was already destroyed after the reaction in region II during the first discharge (see Supporting Information Figure S10). The destruction of the lamellar structures caused in the second region should be responsible for the poor cycling performance in the subsequent cycles.

4. CONCLUSION

In summary, we have demonstrated a facile synthesis of unique lamellar structures of sodium/potassium iron oxide nanosheets via the microwave-assisted process. These lamellar iron oxide layers separated by intercalated sodium/potassium ions possess typical ferromagnetic properties. Owing to their layered feature and high BET surface area, the electrochemical properties of these nanosheets as electrode materials were investigated, showing relatively large initial discharge capacities. Moreover, this facile and fast synthesis strategy may open a new avenue for preparation of other lamellar metal oxide nanomaterials with unique architectures and multifunctionalities.

■ ASSOCIATED CONTENT

Supporting Information. FT-IR spectra, XPS spectra, XRD patterns, and SEM images of the samples (PDF). This material is available free of charge via the Internet at <http://pubs.acs.org>.

■ AUTHOR INFORMATION

Corresponding Author

*Fax: + 86 551 3603040. E-mail: shyu@ustc.edu.cn.

■ ACKNOWLEDGMENT

This work is supported by the National Basic Research Program of China (2010CB934700), the National Natural Science Foundation of China (Nos. 91022032, 50732006), International Science & Technology Cooperation Program of China (2010DFA41170), and the Principle Investigator Award by the National Synchrotron Radiation Laboratory at the University of Science and Technology of China. Liheng Wu thanks Dr. Shaofeng Chen and Yang Lu for helpful discussions

and Linchao Zhang and Xin Fan for their assistance during the electrochemical measurements.

■ REFERENCES

- (1) Armstrong, A. R.; Bruce, P. G. *Nature* **1996**, *381*, 499.
- (2) Takada, K.; Sakurai, H.; Takayama-Muromachi, E.; Izumi, F.; Dilanian, R. A.; Sasaki, T. *Nature* **2003**, *422*, 53.
- (3) Liu, Z. P.; Ma, R. Z.; Osada, M.; Iyi, N.; Ebina, Y.; Takada, K.; Sasaki, T. *J. Am. Chem. Soc.* **2006**, *128*, 4872.
- (4) Chen, C. H.; Crisostomo, V. M. B.; Li, W. N.; Xu, L. P.; Suib, S. L. *J. Am. Chem. Soc.* **2008**, *130*, 14390.
- (5) Peng, H. S.; Tang, J.; Pang, J. B.; Chen, D. Y.; Yang, L.; Ashbaugh, H. S.; Brinker, C. J.; Yang, Z. Z.; Lu, Y. F. *J. Am. Chem. Soc.* **2005**, *127*, 12782.
- (6) Gao, M. R.; Yao, W. T.; Yao, H. B.; Yu, S. H. *J. Am. Chem. Soc.* **2009**, *131*, 7486.
- (7) Chen, D. L.; Sugahara, Y. *Chem. Mater.* **2007**, *19*, 1808.
- (8) Sels, B.; De Vos, D.; Buntinx, M.; Pierard, F.; Kirsch-De Mesmaeker, A.; Jacobs, P. *Nature* **1999**, *400*, 855.
- (9) Choy, J. H.; Kwak, S. Y.; Jeong, Y. J.; Park, J. S. *Angew. Chem., Int. Ed.* **2000**, *39*, 4042.
- (10) Darder, M.; Lopez-Blanco, M.; Aranda, P.; Leroux, F.; Ruiz-Hitzky, E. *Chem. Mater.* **2005**, *17*, 1969.
- (11) Ma, R. Z.; Liu, Z. P.; Takada, K.; Iyi, N.; Bando, Y.; Sasaki, T. *J. Am. Chem. Soc.* **2007**, *129*, 5257.
- (12) Yao, H. B.; Fang, H. Y.; Tan, Z. H.; Wu, L. H.; Yu, S. H. *Angew. Chem., Int. Ed.* **2010**, *49*, 2140.
- (13) Hata, H.; Kobayashi, Y.; Bojan, V.; Youngblood, W. J.; Mallouk, T. E. *Nano Lett.* **2008**, *8*, 794.
- (14) Tagusagawa, C.; Takagaki, A.; Hayashi, S.; Domen, K. *J. Am. Chem. Soc.* **2008**, *130*, 7230.
- (15) Bizeto, M. A.; Shiguihara, A. L.; Constantino, V. R. L. *J. Mater. Chem.* **2009**, *19*, 2512.
- (16) Maeda, K.; Eguchi, M.; Youngblood, W. J.; Mallouk, T. E. *Chem. Mater.* **2009**, *21*, 3611.
- (17) Armstrong, A. R.; Paterson, A. J.; Robertson, A. D.; Bruce, P. G. *Chem. Mater.* **2002**, *14*, 710.
- (18) Lee, S. H.; Kim, T. W.; Park, D. H.; Choy, J. H.; Hwang, S. J.; Jiang, N. Z.; Park, S. E.; Lee, Y. H. *Chem. Mater.* **2007**, *19*, 5010.
- (19) Kim, D. W.; Ko, Y. D.; Park, J. G.; Kim, B. K. *Angew. Chem., Int. Ed.* **2007**, *46*, 6654.
- (20) Tompsett, G. A.; Conner, W. C.; Yngvesson, K. S. *Chem-PhysChem* **2006**, *7*, 296.
- (21) Gerbec, J. A.; Magana, D.; Washington, A.; Strouse, G. F. *J. Am. Chem. Soc.* **2005**, *127*, 15791.
- (22) Buehler, G.; Feldmann, C. *Angew. Chem., Int. Ed.* **2006**, *45*, 4864.
- (23) Ding, K. L.; Miao, Z. J.; Liu, Z. M.; Zhang, Z. F.; Han, B. X.; An, G. M.; Miao, S. D.; Xie, Y. *J. Am. Chem. Soc.* **2007**, *129*, 6362.
- (24) Hu, B.; Wang, S. B.; Wang, K.; Zhang, M.; Yu, S. H. *J. Phys. Chem. C* **2008**, *112*, 11169.
- (25) Yu, J. C.; Hu, X. L.; Li, Q.; Zhang, L. Z. *Chem. Commun.* **2005**, 2704.
- (26) Hu, X. L.; Yu, J. C.; Gong, J. M.; Li, Q.; Li, G. S. *Adv. Mater.* **2007**, *19*, 2324.
- (27) Zhu, Y. J.; Wang, W. W.; Qi, R. J.; Hu, X. L. *Angew. Chem., Int. Ed.* **2004**, *43*, 1410.
- (28) Sun, S. H.; Zeng, H.; Robinson, D. B.; Raoux, S.; Rice, P. M.; Wang, S. X.; Li, G. X. *J. Am. Chem. Soc.* **2004**, *126*, 273.
- (29) Richard-Plouet, M.; Vilminot, S. *J. Mater. Chem.* **1998**, *8*, 131.
- (30) Guillot, M.; Richard-Plouet, M.; Vilminot, S. *J. Mater. Chem.* **2002**, *12*, 851.
- (31) Taibi, M.; Ammar, S.; Jouini, N.; Fievet, F.; Molinier, P.; Drillon, M. *J. Mater. Chem.* **2002**, *12*, 3238.
- (32) Poizot, P.; Laruelle, S.; Grugeon, S.; Dupont, L.; Tarascon, J. M. *Nature* **2000**, *407*, 496.
- (33) Cao, A. M.; Hu, J. S.; Liang, H. P.; Wan, L. J. *Angew. Chem., Int. Ed.* **2005**, *44*, 4391.

- (34) Reddy, A. L. M.; Shaijumon, M. M.; Gowda, S. R.; Ajayan, P. M. *Nano Lett.* **2009**, *9*, 1002.
- (35) Zhan, F. M.; Geng, B. Y.; Guo, Y. J. *Chem.—Eur. J.* **2009**, *15*, 6169.
- (36) Zhang, W. M.; Wu, X. L.; Hu, J. S.; Guo, Y. G.; Wan, L. J. *Adv. Funct. Mater.* **2008**, *18*, 3941.
- (37) Cui, Z. M.; Hang, L. Y.; Song, W. G.; Guo, Y. G. *Chem. Mater.* **2009**, *21*, 1162.